Supporting Information

Redox-responsive degradable honeycomb manganese oxide nanostructures as an effective nanocarrier for intracellular glutathione-triggered drug release

Dinggeng He, Xiaoxiao He, Kemin Wang,* Xue Yang, Xiaoxiao Yang, Zhen Zou and Xuecai Li*

State Key Laboratory of Chemo/Biosensing and Chemometrics, College of Chemistry and Chemical Engineering, College of Biology, Key Laboratory for Bio-Nanotechnology and Molecular Engineering of Hunan Province, Hunan University, Changsha 410082, P. R. China.

Experimental details

Materials

Potassium permanganate ($KMnO_4$) and oleic acid (OA) were purchased from Alfa Aesar. Glutathione (GSH), 3-(4,5-dimethylthialzol-2-yl)-2,5-diphenyltetrazolium bromide (MTT), alpha lipoic acid (ALA), buthionine sulfoximine (BS) and N-ethylmaleimide (NEM) were purchased from Sigma-Aldrich. Doxorubicin hydrochloride (DOX) was purchased from Dingguo reagent company (Beijing, China). All buffers were prepared with ultra-pure MilliQ water (resistance >18.2 MΩ cm^{-1}). Other chemicals were used as received without further purification.

Preparation of $hMnO_2$ nanostructures

In a typical procedure, 0.5 g of $KMnO_4$ was dissolved in 250 mL of distilled water, and the mixture was fleetly stirred for about 0.5 h. A total of 5.0 mL of OA was then added. The resulting mixture was reacted for 48 h and a crude brown-black product was collected by centrifugation, washed several times with deionized water and alcohol to remove any possible residual reactants. The purified $hMnO_2$ was redispersed in 250 mL of deionized water. In this process, OA in aqueous solution formed a steady oil/water emulsion, which directed the synthesis of $hMnO_2$ materials in the presence of $KMnO_4$ as the Mn precursor. Some small MnO_2 nuclei were first produced at the oil/water interface via the redox reaction between $KMnO_4$ and OA. Then, MnO_2 nuclei continually grew into lamellar MnO_2 platelets, ultimately resulting in the formation of $hMnO_2$ nanostructures.

Drug loading and release

24 mL of $hMnO_2$ aqueous solution (0.5 mg mL^{-1}) was mixed with 1 mL of DOX aqueous solution (2 mg mL^{-1}), and stirred at room temperature for 15 h. In this process, DOX was successfully adsorbed onto the basal plane of $hMnO_2$ by physisorption to form $hMnO_2$-DOX. The amount of adsorbed drug was determined from the difference between the starting amount of DOX and the amount determined by measuring the absorbance of the

drug from the supernatant liquid at 490 nm in PBS buffer solution, quantified from a standard curve. Afterwards, $hMnO_2$-DOX (0.1 mg mL^{-1}) was decomposed in all kinds of GSH solution with different concentrations and treated for different times. The DOX release was measured at different time intervals by fluorescence emission spectroscopy at 570 nm to determine the drug releasing kinetics.

Cell imaging

Hepatocellular carcinoma HepG2 and normal liver cell line L02 were maintained at 37 °C in 5% CO_2 in RPMI media. The cells were plated at around 60-70% confluency 24 h before imaging experiments in 35-mm culture dishes. Prior to imaging experiments, the HepG2 cells and L02 cells were treated with BS (100 μM) for 1 h and ALA (500 μM) for 24 h, respectively. To decrease GSH concentration in living cells, untreated HepG2 and ALA-pretreated L02 cells were treated with NEM (500 μM) for 20 min. Both cell lines were washed for three times with cell culture media and incubated with $hMnO_2$-DOX (20 μg mL^{-1}) for 3h. The cell lines were further washed using cell culture media and subsequently imaged at ambient temperature.

Cell viability measurements

The cytotoxicity was evaluated by MTT assays in HepG2 cells and L02 cells. The MTT solution was filtered through a 0.22 μm filter and stored at 4 °C. The testing procedures was carried out as follows: HepG2 cells and L02 cells were respectively seeded at 1×10^4 cells per cell into a 96-well cell culture plate in RMPI with 10% FBS at 37 °C and with 5% CO_2 for 24 h. Then, the culture medium was replaced with freshly prepared medium containing with various concentrations of $hMnO_2$-DOX or free DOX and sequentially incubated for another 24 h. Similarly, the single $hMnO_2$ with different concentrations and Mn^{2+} ions ($MnCl_2$) with corresponding concentrations to Mn content of $hMnO_2$ were incubated with HepG2 cells and L02 cells for 48 h, respectively. After that time, cells were incubated with the medium containing 100 μL fresh RMPI with 10% FBS and MTT (20 μL, 5 mg mL^{-1} in PBS). Cells were cultured for another 4 h at 37 °C. Finally, the medium was removed and the formazan crystals were dissolved with dimethyl sulfoxide (DMSO, 150 μL). The assays were performed according to the manufacturer's instructions. The absorbance of MTT at the wavelength of 570 nm was measured.

Characterizations

Transmission electron microscopy (TEM) and energy dispersive spectroscopy (EDS) measurements carried out on a JEOL 3010 transmission electron microscope operating at an acceleration voltage of 100 kV. Field-emission scanning electron microscopy (FE-SEM) was performed with a JSM-6700F microscope. Powder X-ray diffraction (XRD) patterns of as-prepared samples were recorded on a Scintag XDS-2000 powder diffractometer using Cu Kα irradiation (λ = 0.154 nm). The 2θ range and recording step were 5−80° and 0.004°, respectively. Crystallite size was calaulated using the Scherrer equation. N_2 adsorption−desorption isotherms were obtained at −196 °C on a Micromeritics ASAP 2010 sorptometer by static adsorption procedures. Samples were degassed at 100 °C and 10^{-3} Torr for a minimum of 12 h prior to analysis. Brunauer−Emmett−Teller (BET) surface areas were calculated from the linear part of the BET plot according to IUPAC recommendations. Pore size distribution was estimated from the adsorption branch of the isotherm by the Barrett−Joyner−Halenda (BJH) method. The zeta potential of nanomaterials was measured at 25 °C using a Nano ZS90 laser particle analyzer, Malvern Instruments, UK. UV-vis spectra were collected using a DU-800 spectrophotometer. All fluorescence spectra were recorded on a Hitachi F4500 FL spectrophotometer. Fourier transform infrared (FTIR) spectra were obtained from a TENSOR 27 spectrometer, Bruker Instruments Inc., Germany. Photographs were taken with a digital camera. Confocal laser scanning microscopy (CLSM) images were obtained on a Fluoview FV500, Olympus. The MTT assays were obtained by a multi-detection microplate reader.

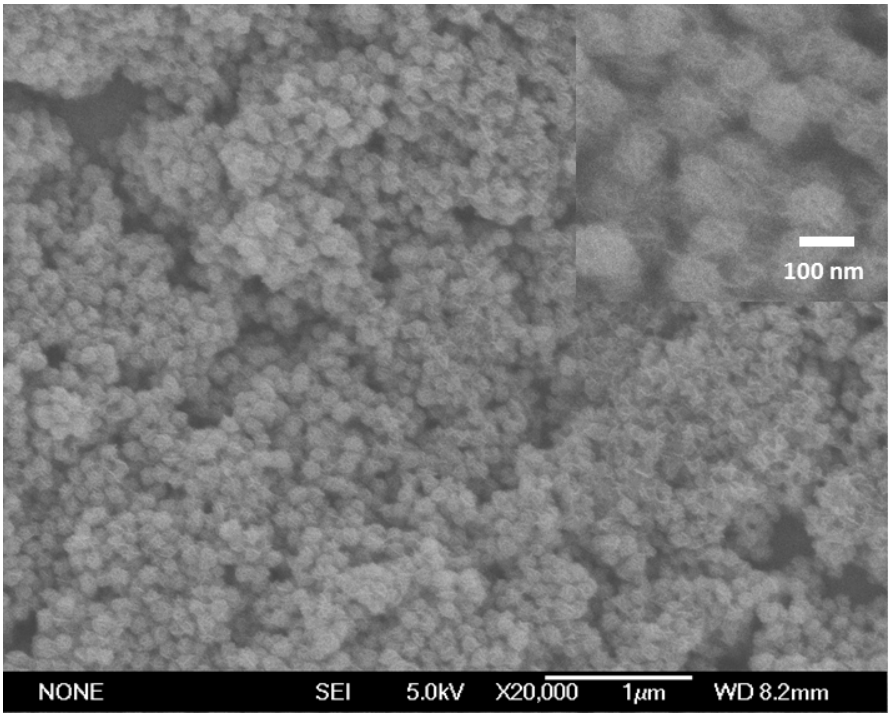

Fig. S1 FE-SEM images of as-prepared $hMnO_2$. The inset is a magnified SEM image.

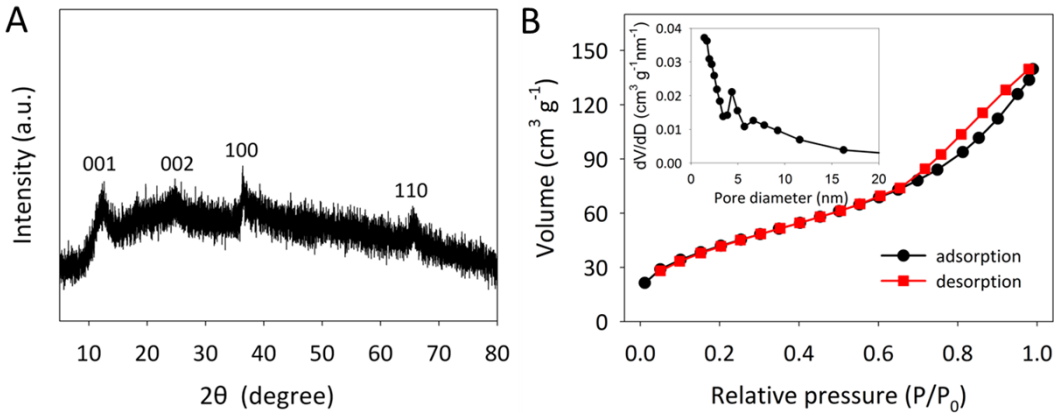

Fig. S2 (A) XRD patterns of $hMnO_2$ nanostructures. (B) Nitrogen sorption isotherms and pore size distributions (inset) of $hMnO_2$ nanostructures.

The crystallographic structure of the $hMnO_2$ was further studied by powder X-ray diffraction (XRD). The XRD analysis of $hMnO_2$ showed four significant peaks at 2θ = 12.16, 24.25, 36.49, and 65.81°, which could be assigned to the (001), (002), (100), and (110) planes of birnessite-type MnO_2, respectively. According to the (001) reflection, the thickness of laminar MnO_2 platelet was estimated to be 7.9 nm by the Scherrer equation. Thus, the MnO_2 platelet was supposed to consist of about seven MnO_2 monolayers.

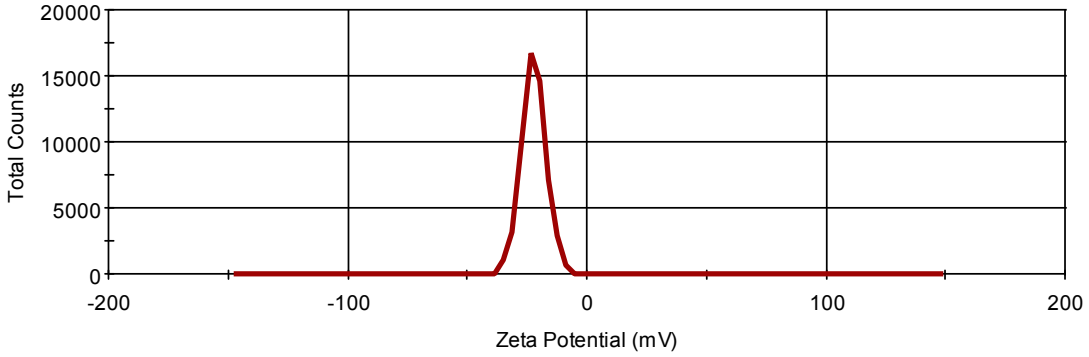

Fig. S3 Zeta potential of as-prepared $hMnO_2$ nanostructures. The zeta potential of $hMnO_2$ is −22.1 eV in water.

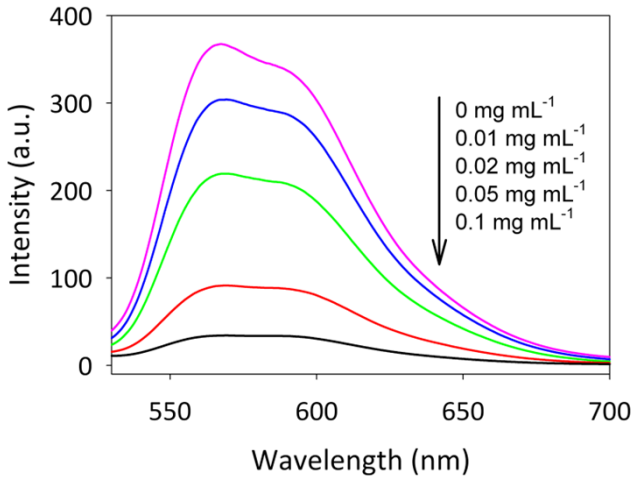

Fig. S4 Fluorescence emission spectra of DOX after treatment with $hMnO_2$ at different concentrations.

The fluorescence quenching of DOX was dependent on the concentration of $hMnO_2$. In the presence of a small amount (0.1 mg mL^{-1}) of $hMnO_2$, the fluorescence of DOX (20 μM) was almost completely quenched, indicating a high quenching efficiency of $hMnO_2$.

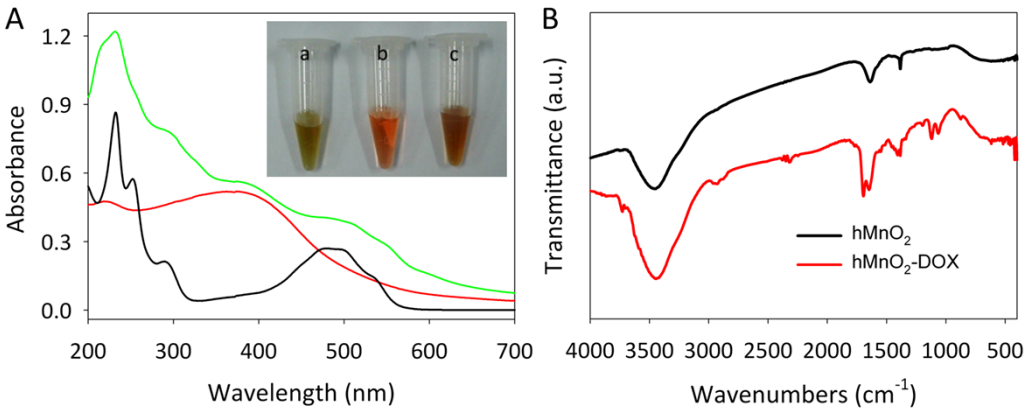

Fig. S5 (A) UV-vis absorption spectra of free DOX (black line), $hMnO_2$ (red line) and $hMnO_2$-DOX (green line). Inset: Photographs of aqueous solutions of $hMnO_2$ (a), free DOX (b) and $hMnO_2$-DOX (c). (B) Corresponding FT-IR spectra of $hMnO_2$ and $hMnO_2$-DOX.

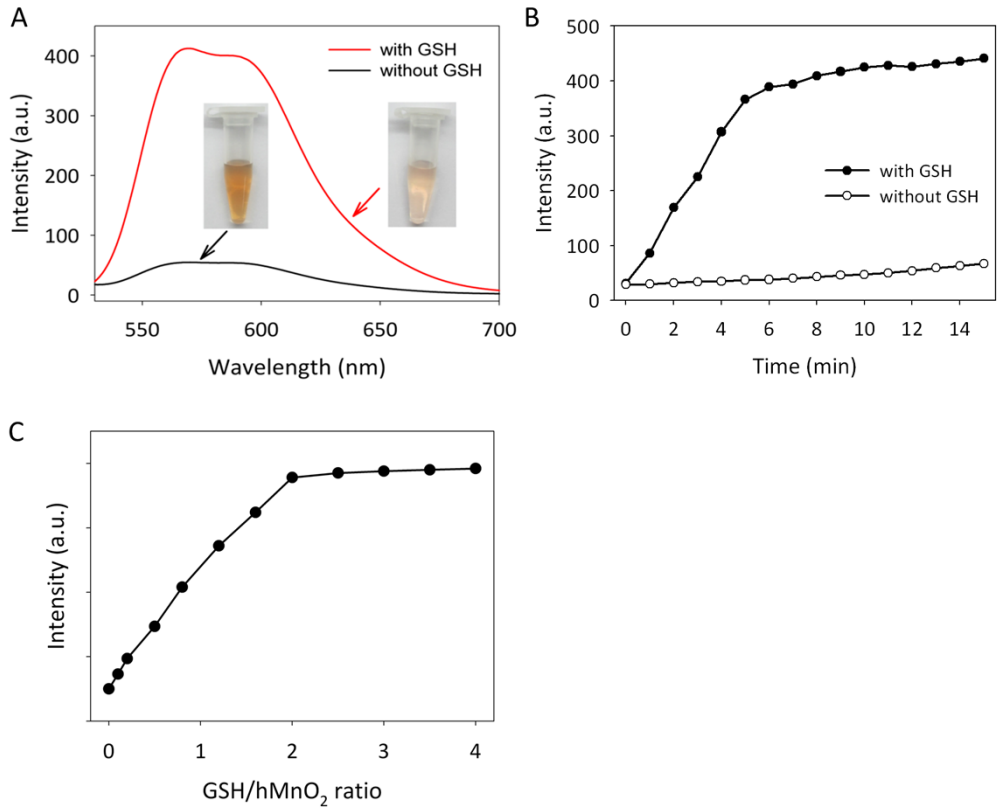

Fig. S6 (A) Fluorescence emission spectra and photographs (inset) of $hMnO_2$-DOX solution (0.05 mg mL^{-1}) after being treated with and without GSH molecules (1 mM) (λ_{ex}= 488 nm). (B) Time dependence of fluorescence intensity at 570 nm for the $hMnO_2$-DOX solution in the presence or absence of GSH. (C) Plot of fluorescence intensity at 570 nm against the GSH/$hMnO_2$ molar ratio.

During this redox reaction, GSH was oxidized to generate glutathione disulfide (GSSG) through thiol-disulfide exchange as shown in eq 1.

$$MnO_2 + 2GSH + 2H^+ \rightarrow Mn^{2+} + GSSG + 2H_2O \quad (1)$$

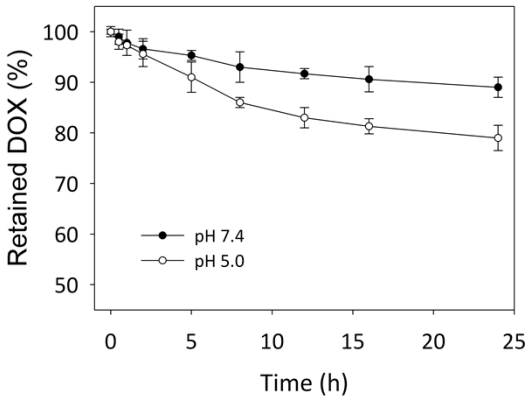

Fig. S7 Drug release from $hMnO_2$-DOX as the function of time at pH 7.4 and 5.0.

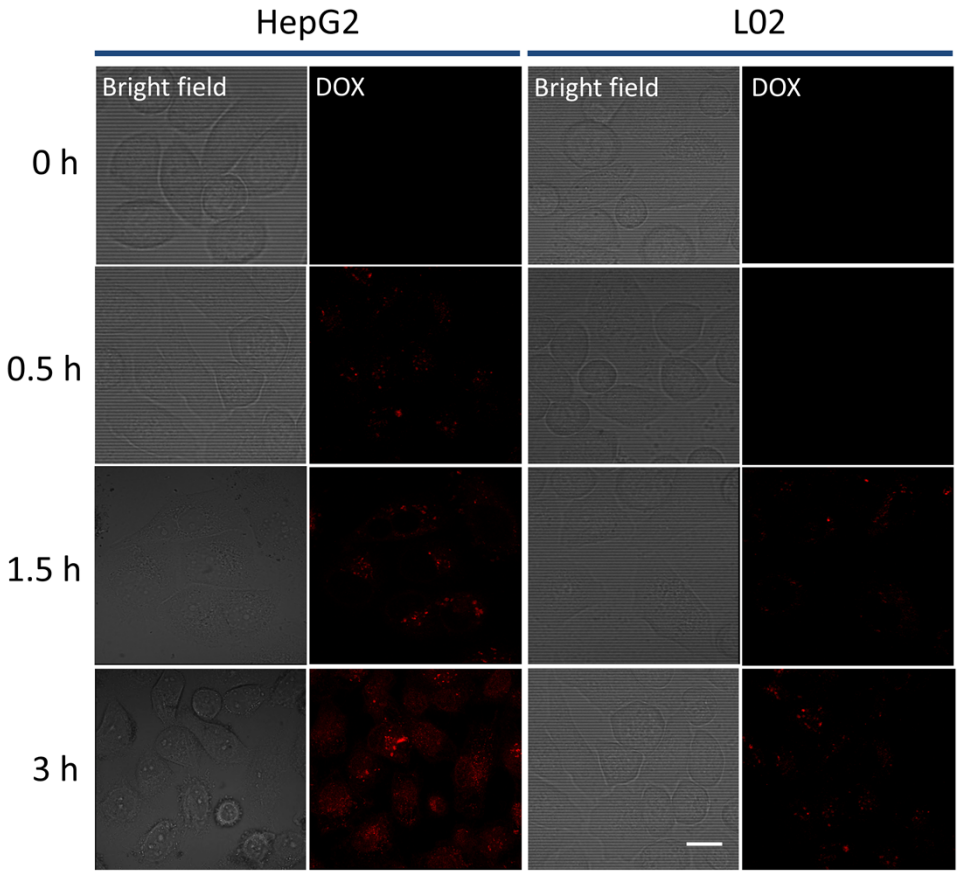

Fig. S8 CLSM images of HepG2 cells and L02 cells treated with $hMnO_2$-DOX (20 μg mL^{-1}) at different times (0, 0.5, 1.5, and 3 h). Scale bar: 20 μm.

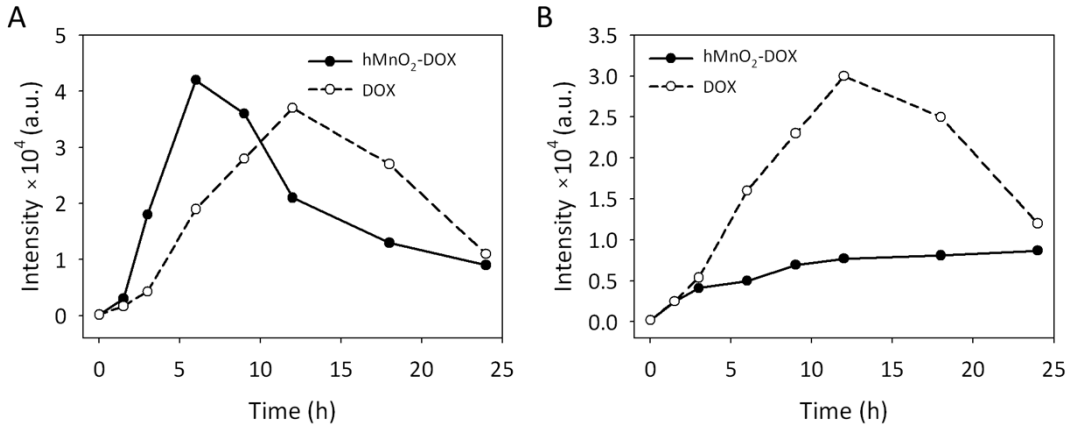

Fig. S9 Time-dependent intracellular fluorescence emissions from HepG2 cells (A) and L02 cells (B) treated with $hMnO_2$-DOX (20 μg mL^{-1}) and free DOX molecules (2 μg mL^{-1}). The intracellular fluorescence intensities were measured using a fluorescence microtiter plate reader at different time points.

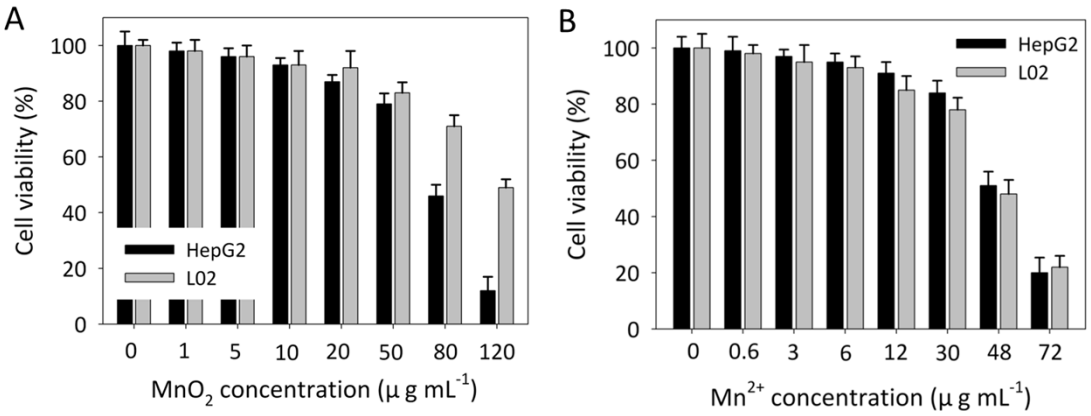

Fig. S10 Viability of HepG2 cells and L02 cells after incubation with different concentrations of $hMnO_2$ (A) and Mn^{2+} ions (B) for 48 h. The amount of Mn^{2+} ions corresponds to the Mn content of $hMnO_2$.